Journal of Power Sources 271 (2014) 455–464

Contents lists available at ScienceDirect

Journal of Power Sources

journal homepage: www.elsevier.com/locate/jpowsour

Molecular design of the diketopyrrolopyrrole-based dyes with varied donor units for efficient dye-sensitized solar cells

Xu-Feng Zang [a], Zu-Sheng Huang [a], Han-Lun Wu [a], Zafar Iqbal [b], Lingyun Wang [a], Herbert Meier [c], Derong Cao [a, *]

[a] School of Chemistry and Chemical Engineering, State Key Laboratory of Luminescent Materials and Devices, South China University of Technology, Guangzhou 510641, China
[b] Applied Chemistry Research Centre, PCSIR Laboratories Complex, Lahore 54000, Pakistan
[c] Institute of Organic Chemistry, University of Mainz, Mainz 55099, Germany

HIGHLIGHTS

- Diketopyrrolopyrrole-based dyes with phenyl as additional π-bridge were designed.
- Donor linking directly to DPP leads to a better delocalization of the excited state.
- The position and number of phenyl unit influence the properties of the dyes.
- Triphenylamine as donor causes better performance than phenothiazine as donor.
- The DSSC based on the dye with triphenylamine as donor showed a PCE of 8%.

GRAPHICAL ABSTRACT

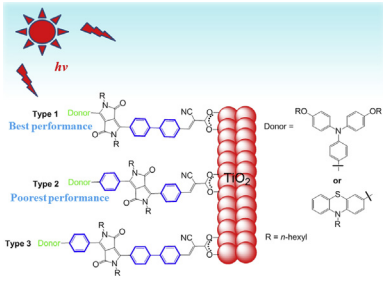

ARTICLE INFO

Article history:
Received 15 May 2014
Received in revised form
6 August 2014
Accepted 7 August 2014
Available online 15 August 2014

Keywords:
Dye-sensitized solar cells
Organic dye
Diketopyrrolopyrrole
π-Bridge
Triphenylamine
Phenothiazine

ABSTRACT

Three types of novel diketopyrrolopyrrole-based organic dyes (**Type 1**–**3**) with phenyl unit as an additional π-bridge and triphenylamine or phenothiazine as the donors are designed and synthesized for dye-sensitized solar cells (DSSCs). **Type 1** dyes incorporating the donor segment directly to the diketopyrrolopyrrole core lead to a better electron communication between the donor and acceptor, allowing an efficient charge transfer process. **Type 2** and **Type 3** dyes with a phenyl unit between the donor and diketopyrrolopyrrole unit show lower delocalization of the excited state. Compared with **Type 3** dyes, **Type 1** dyes exhibit higher conjugated skeleton co planarity and shorter electron transfer distance from the donor to TiO_2, resulting in the red-shifts of absorption and promotion of electron injection, respectively. Moreover, the dyes with triphenylamine as the donor display better UV performance and lower trend of aggregation than the dyes with phenothiazine as the donor. Finally, a power conversion efficiency of 8% with chenodeoxycholic acid as the co-absorbant for the DSSC based on **Type 1** dyes with triphenylamine is achieved. The results reveal that the donors, the position and number of phenyl unit of the dyes significantly influence the photovoltaic performance of their DSSCs.

* Corresponding author. Tel.: +86 20 87110245; fax: +86 20 87110245.
E-mail address: drcao@scut.edu.cn (D. Cao).

http://dx.doi.org/10.1016/j.jpowsour.2014.08.030
0378-7753/

1. Introduction

Since Grätzel and O'Regan reported the pioneer work in 1991, ever-increasing researchers focus their attention on dye-sensitized solar cells (DSSCs) due to their high performance and low-cost [1–3]. As a promising class of sensitizers, metal-free organic dyes have been well developed because of their higher molar extinction coefficient, less environmental issues and more variable structure adjustability in comparison with the heavy metal based organic dyes [4,5]. However, there are certain bottlenecks such as shorter lifetime of excitons at excited states and relatively narrow absorption in the visible region [6,7]. Even though a remarkable progress has been made in organic dyes, further optimization of their chemical structures is still of great necessity. It is well known that diketopyrrolopyrrole (**DPP**) chromophore has been extensively used in pigments due to its strong electron-withdrawing ability, exceptional photochemical, weather and heat stability [8]. The efficient intramolecular charge transfer of **DPP** allows a broad and intense spectral absorption in the visible light region [9]. Consequently, it has been suggested as a promising π-conjugated unit for organic dyes because it is expected to overcome the above drawbacks of metal-free organic dyes. However, only a few reports on **DPP**-based organic dyes are available [8,10]. Therefore it should attract more scientific attention.

Moreover, among these finite reported **DPP**-based sensitizers for DSSCs, just a few dyes exhibit promising power conversion efficiency [11–14]. According to the previous reports, the possible major reasons which curtail their efficiencies may be attributed to the serious π-π staking, inappropriate energy level alignment and relative weak light-harvesting ability in the shorter wavelength (such as the range of 400–550 nm) [8,15–17]. It is well known that **DPP** is a very planar framework which always readily causes a strong π-π intermolecular interaction [16,18,19]. As mentioned, although most of these reported **DPP**-based dyes show broad-range light absorption in longer wavelength even extending to near infra-red (NIR) region, their device performances are usually not as good as expected. Tian and coworkers found that when employing three thiophene units as an additional π-bridge in one **DPP**-based dye molecule (**DPP–II**), the absorption range is largely shifted to the longer wavelength, which evidently limits its performance [8]. Besides, the lowest unoccupied molecular orbital (LUMO) energy level of **DPP–II** is remarkably positive-shifted to −0.56 V *vs.* NHE. Since the bottom of the conduction band of TiO_2 is −0.50 V *vs.* NHE, the driving force for electron injection process from the excited dye molecule to TiO_2 may not be enough. In fact, a big energy gap between the LUMO level of the dye and TiO_2 conduction band, or a large gap between the highest occupied molecular orbital (HOMO) level of the dye and potential of the redox couple, which may both cause an energy loss, leading to a low DSSC efficiency [20]. So, tuning the suitable HOMO and LUMO levels of the dye is extremely necessary.

In order to overcome these disadvantageous features, it is necessary to study the effects of the position and number of phenyl units as additional π-bridge as well as the different donors on the photovoltaic performance of the diketopyrrolopyrrole-based dyes. Thus, we designed three types of novel organic dyes (**Type 1–3**) with **DPP** as a π-bridge and phenyl unit as an additional π-bridge (Fig. 1). As shown in Fig. 1, **Type 1** dyes incorporated the donor segment directly to the diketopyrrolopyrrole core without an additional phenyl unit between the donor and **DPP** unit, while **Type 2** and **Type 3** dyes with a phenyl unit between the donor and **DPP** unit and a phenyl or biphenyl unit between the **DPP** and acceptor unit, respectively. The introduction of 10-hexyl-10*H*-phenothiazine (**PTZ**) and 4-(hexyloxy)-*N*-(4-(hexyloxy)phenyl)-*N*-phenylaniline (**TPA**) as the donor parts to **Type 1–3** dyes gave two series of dyes **PTZ1-3** and **TPA1-3**, respectively. The molecular structures of the dyes were designed according to the following considerations. Firstly, an *n*-hexane group was employed as a barrier both on the **DPP** and electron donor unit, which could not only surmount the solubility problem, but also retard I_3^- ions to approach TiO_2 surface and prevent the formation of dye aggregation [21,22]. Secondly, a phenyl unit with high steric hindrance was used instead of the planar π-bridge (i.e. thiophene and furan) to twist the structure framework [18], controlling the planarity of the molecule to reduce the undesirable aggregation. Thirdly, **PTZ** and **TPA** were utilized as the donor units to tune the HOMO and LUMO energy levels. **PTZ** has been considered as one of the promising donor moieties of organic dyes due to its high electrochemical stability and electron-donating ability [23–27]. **TPA** is a relatively chemical stable structure and its twisted/screw-like configuration can impede the aggregation [28–30]. To the best of our knowledge, **DPP**-based dyes with **PTZ** as an electron donor have not been reported. Introduction of phenyl unit as another π-bridge besides **DPP** may alter the energy level, too. As compared to the high polarizability and electron rich

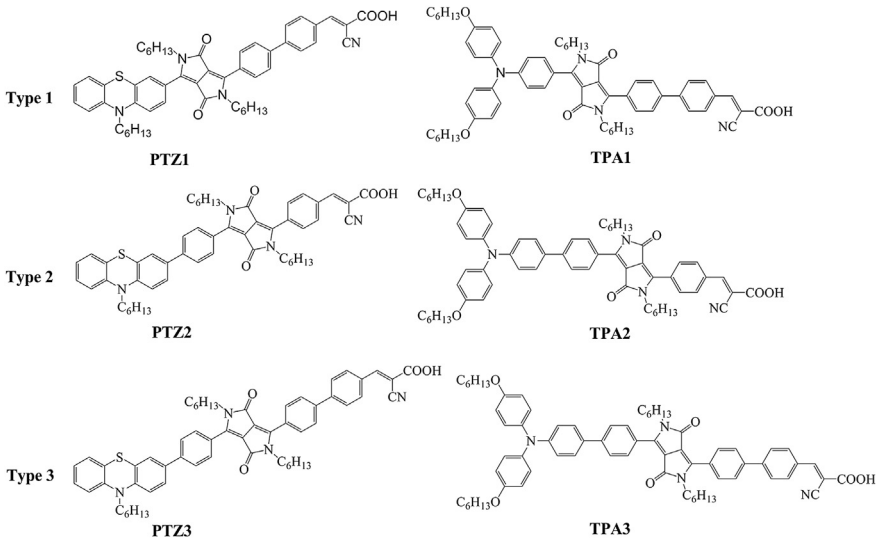

Fig. 1. Structures of the dyes **PTZ1–3** and **TPA1–3**.

π-bridge (i.e. thiophene and furan), phenyl unit makes the LUMO level negative-shift [8,31–33]. Fourthly, the influence of the position of phenyl units on the performance of the dyes and DSSCs was studied. Finally, **Type 3** dyes were synthesized as a reference to investigate the effect of the π-bridge length on the photovoltaic properties of the DSSCs.

2. Experimental section

2.1. Materials

All chemicals and reagents were purchased from J&K, Adamas and Darui, and used as received. Reagent grade solvents like DMF and 1,2-dichloroethane were dried over 4A molecular sieve, while toluene was distilled under an atmosphere of argon before use. Other solvents were purchased from commercial suppliers and used without further purification.

2.2. Analytical measurements

^{1}H NMR and ^{13}C NMR spectra were recorded on 400 MHz Bruker Advance spectrometer using $CDCl_3$ or THF-d_8 as solvent. Melting points were taken on Tektronix X4 microscopic melting point apparatus and uncorrected. HRMS spectra were obtained by Agilent Technologies 1290 Infinity mass spectroscopy. The absorption spectra of the dye solutions were obtained in dichloromethane (DCM) solution (2×10^{-5} M) by using a Shimadzu UV-2450 spectrophotometer, and the emission spectra were obtained in DCM solution (2×10^{-5} M) by Fluorolog *III* photoluminescence spectrometer. The oxidation potential of dyes adsorbed on TiO_2 films was measured by cyclic voltammetry on an electrochemistry workstation (e-corder (ED 401) potentiostat) with a three-electrode cell. The dye coated TiO_2 films were utilized as a working electrode. Ag/AgCl in KCl (3 M) solution and an auxiliary platinum wire were utilized as reference and counter electrodes. 0.1 M $TBAPF_6$ in acetonitrile was used as the supporting electrolyte. The potential of the working electrode was calibrated by an Fc/Fc^+ couple as internal reference. Photocurrent–voltage characteristics were performed on a Keithley 2400 source meter under simulated AM 1.5G illumination (100 mW cm^{-2}) provided by solar simulator (Pecell-L15, Japan). Incident photon-to-current conversion efficiency (IPCE) spectra were carried out on a PEC-S20 action spectrum measurement system. Electrochemical impedance spectroscopy (EIS) measurements were carried out on a Zahner elektrik electrochemical workstation under the dark condition. The data were analyzed by Z-view software.

2.3. Fabrication of the dye-sensitized solar cells

Nanocrystalline TiO_2 films (12 μm in thickness) with a transparent layer (15 μm) and a scattering layer (4 μm) in thickness were prepared by a screen printing technique, followed by sintering at 450 °C under an air flow. After cooling, the TiO_2 films were soaked in a 0.05 M aqueous $TiCl_4$ solution for 30 min at 70 °C, and then rinsed in deionized water and ethanol. The $TiCl_4$-treated TiO_2 films were annealed at 450 °C for 30 min, and then cooled to 100 °C before being dipped into a 3.0×10^{-4} M solution of dyes in DCM for 24 h at room temperature. After adsorption of the dyes, the electrodes were rinsed in DCM. The resulting photoelectrode and Pt-counter electrodes were assembled into a sealed sandwich solar cell with a thermoplastic frame. The electrolyte (0.6 M 1-methyl-3-propylimidazolium iodide (PMII), 0.10 M guanidinium thiocyanate, 0.05 M LiI, 0.07 M I_2 and 0.5 M tert-butylpyridine in acetonitrile/valeronitrile (85:15)) was injected from a hole made on the counter electrode into the interspace between the photoanode and counter electrode. The active area of the dye coated TiO_2 film was 0.16 cm^2.

2.4. Synthesis

2.4.1. 10-Hexyl-10H-phenothiazine-3-carbonitrile (**2**)

A mixture of 10-hexyl-10*H*-phenothiazine-3-carbaldehyde (**1**) (2.05 g, 7.05 mmol), hydroxyamine hydrochloride (0.58 g, 8.45 mmol), acetic acid (1.44 g, 24.00 mmol) and pyridine (0.84 g, 10.58 mmol) in DMF (25 mL) was stirred and heated to 138 °C for 3.5 h under argon atmosphere. After cooling to room temperature, the reaction was quenched by water and the mixture was extracted with CH_2Cl_2. The organic layer was dried with anhydrous Na_2SO_4 and the solvent was removed by rotary evaporation. The crude product was further purified by column chromatography (silica gel, petroleum ether (bp 60–90 °C)/ethyl acetate = 60/1, v/v) to give **2** as a light yellow liquid (1.93 g, 6.70 mmol) in 95.1% yield. ^{1}H NMR ($CDCl_3$, 400 MHz, ppm): δ 7.34–7.32 (m, 1H), 7.20–7.18 (m, 1H), 7.16–7.14 (m, 1H), 7.07–7.05 (m, 1H), 6.97–6.93 (m, 1H), 6.87–6.85 (m, 1H), 6.78–6.76 (m, 1H), 3.81 (t, J = 7.2 Hz, 2H), 1.79–1.72 (m, 2H), 1.45–1.37 (m, 2H), 1.32–1.27 (m, 2H), 0.89–0.86 (m, 3H). ^{13}C NMR ($CDCl_3$, 100 MHz, ppm): δ 149.1, 143.4, 131.5, 130.1, 127.7, 127.5, 125.5, 123.5, 123.2, 118.8, 116.0, 115.0, 104.9, 47.7, 31.3, 26.5, 26.4, 22.5, 13.9. HRMS (ESI, m/z): $[M + H]^+$ calcd for ($C_{19}H_{21}N_2S$): 309.1420, found: 309.1417.

2.4.2. 3-(4-Bromophenyl)-2,5-dihexyl-6-(10-hexyl-10H-phenothiazin-3-yl)pyrrolo[3,4-c]pyrrole-1,4(2H,5H)-dione (**10a**)

A mixture of sodium (437 mg, 19.00 mmol) with $FeCl_3$ as catalyst in *tert*-amyl alcohol (35 mL) was stirred and heated to 100 °C under argon atmosphere until sodium was dissolved. After cooling to room temperature, ethyl 2-(4-bromophenyl)-5-oxo-4,5-dihydro-1*H*-pyrrole-3-carboxylate (**8**) (1.55 g, 5.00 mmol) and **2** (2.00 g, 6.50 mmol) were added. The mixture was kept stirring at 80 °C for 20 h. Then the mixture was cooled to room temperature and poured into ice water. Acetic acid (5 mL) was added. Then it was diluted with methanol (50 mL). The precipitate was filtered, washed with water and acetone, and dried in vacuo at 60 °C to give **9a** as a dark-red solid. **9a** does not dissolve in most deuterated solvents. Therefore it was not characterized by NMR spectra and was reacted in the next step directly.

A mixture of **9a** (1.80 g, 3.14 mmol) and potassium *tert*-butanolate (0.88 g, 7.85 mmol) in *N*-methyl-2-pyrrolidone (**NMP** (30 mL)) was stirred and heated to 60 °C for 1 h under argon atmosphere. 1-Bromohexane (4.13 g, 25.00 mmol) in 7 mL of **NMP** was added dropwise, and the mixture was kept stirring for another 24 h. After cooling to room temperature, the mixture was poured into water and extracted with CH_2Cl_2. The organic layer was dried with anhydrous Na_2SO_4 and the solvent was removed by rotary evaporation. The crude product was further purified by column chromatography (silica gel, petroleum ether (bp 60–90 °C)/ethyl acetate = 30/1, v/v) to give **10a** as a light orange solid (mp 149–151 °C) (1.67 g, 2.25 mmol) in 33.6% yield for the two step reactions. ^{1}H NMR ($CDCl_3$, 400 MHz, ppm): δ 7.78–7.75 (m, 1H), 7.67–7.60 (m, 4H), 7.55–7.54 (m, 1H), 7.16–7.08 (m, 2H), 6.95–6.85 (m, 3H), 3.86 (t, J = 7.2 Hz, 2H), 3.76–3.70 (m, 4H), 1.86–1.79 (m, 2H), 1.62–1.53 (m, 4H), 1.47–1.41 (m, 2H), 1.33–1.31 (m, 4H), 1.26–1.20 (m, 12H), 0.91–0.87 (m, 3H), 0.84–0.81 (m, 6H). ^{13}C NMR ($CDCl_3$, 100 MHz, ppm): δ 162.9, 162.4, 148.4, 147.9, 145.6, 143.7, 132.2, 130.2, 129.1, 127.6, 127.5, 127.4, 127.1, 125.3, 124.5, 123.7, 123.3, 121.9, 115.7, 114.9, 110.2, 108.8, 48.0, 42.2, 41.9, 31.5, 31.3, 31.3, 29.8, 29.5, 29.5, 26.8, 26.7, 26.5, 26.5, 22.7, 22.6, 22.5, 14.7, 14.0. HRMS (ESI, m/z): $[M + H]^+$ calcd for ($C_{42}H_{51}^{79}BrN_3O_2S$): 740.2880, found: 740.2883; $[M + H]^+$ calcd for ($C_{42}H_{51}^{81}BrN_3O_2S$): 742.2867, found: 742.2860.

*2.4.3. 4′-(2,5-Dihexyl-4-(10-hexyl-10H-phenothiazin-3-yl)-3,6-dioxo-2,3,5,6-tetrahydropyrrolo[3,4-c]pyrrol-1-yl)-[1,1′-biphenyl]-4-carbaldehyde (**11a**)*

A mixture of **10a** (0.25 g, 0.34 mmol), 4-formylphenylboronic acid (66.00 mg, 0.44 mmol), $Pd(PPh_3)_4$ (32 mg, 0.03 mmol), and 2 M aqueous solution of K_2CO_3 (0.35 mL) in redistilled toluene (40 mL) was stirred and heated to 80 °C under argon atmosphere for 24 h. After cooling to room temperature, the reaction was quenched by water and the mixture was extracted with CH_2Cl_2. The organic layer was dried with anhydrous Na_2SO_4 and the solvent was removed by rotary evaporation. The crude product was further purified by column chromatography (silica gel, petroleum ether (bp 60–90 °C)/ethyl acetate = 10/1, v/v) to give **11a** as an aubergine solid (mp 127–129 °C) (0.22 g, 0.29 mmol) in 85.4% yield. ^{1}H NMR ($CDCl_3$, 400 MHz, ppm): δ 10.01 (s, 1H), 7.92–7.88 (m, 4H), 7.77–7.71 (m, 5H), 7.56–7.55 (m, 1H), 7.13–7.06 (m, 2H), 6.92–6.85 (m, 2H), 6.80–6.78 (m, 1H), 3.80–3.73 (m, 6H), 1.81–1.74 (m, 2H), 1.62–1.59 (m, 4H), 1.43–1.37 (m, 2H), 1.31–1.28 (m, 4H), 1.27–1.20 (m, 12H), 0.89–0.86 (m, 3H), 0.84–0.79 (m, 6H). ^{13}C NMR ($CDCl_3$, 100 MHz, ppm): δ 191.7, 162.8, 162.4, 148.1, 147.6, 146.1, 145.7, 143.5, 141.6, 135.6, 130.3, 129.4, 129.1, 128.4, 127.6, 127.5, 127.5, 127.4, 127.0, 124.2, 123.4, 123.1, 121.8, 115.5, 114.7, 110.2, 108.8, 47.9, 42.1, 42.0, 31.4, 31.3, 29.5, 29.4, 26.6, 26.4, 22.6, 22.5, 22.5, 14.0, 14.0. HRMS (ESI, *m*/*z*): $[M + H]^+$ calcd for ($C_{49}H_{56}N_3O_3S$): 766.4037, found: 766.4037.

*2.4.4. 4-(4-(4-Bromophenyl)-2,5-dihexyl-3,6-dioxo-2,3,5,6-tetrahydropyrrolo[3,4-c]pyrrol-1-yl)benzaldehyde (**14**)*

A mixture of **13** (1.00 g, 1.65 mmol) and 2 M aqueous solution of hydrochloric acid (10 mL) in THF (20 mL) was stirred and heated to 80 °C for 2 h. After cooling to room temperature, the mixture was poured into ice water. The precipitate was collected and dried to give **14** as a red solid (mp 115–117 °C) (0.88 g, 1.56 mmol) in 94.5% yield. ^{1}H NMR ($CDCl_3$, 400 MHz, ppm): δ 10.06 (s, 1H), 7.90–7.84 (m, 4H), 7.61–7.59 (m, 2H), 7.52–7.50 (m, 2H), 3.73–3.66 (m, 4H), 1.46–1.43 (m, 4H), 1.24–1.16 (m, 12H), 0.84–0.76 (m, 6H). ^{13}C NMR ($CDCl_3$, 100 MHz, ppm): δ 190.2, 161.3, 161.1, 147.5, 145.6, 136.4, 132.4, 131.0, 129.2, 128.8, 128.2, 125.6, 125.1, 109.8, 108.77, 40.69, 30.1, 30.1, 28.2, 25.3, 21.4, 12.9. HRMS (ESI, *m*/*z*): $[M + H]^+$ calcd for ($C_{31}H_{36}^{79}BrN_2O_3$): 563.1904, found: 563.1908; $[M + H]^+$ calcd for ($C_{31}H_{36}^{81}BrN_2O_3$): 565.1889, found: 565.1890.

*2.4.5. (E)-2-Cyano-3-(4′-(2,5-dihexyl-4-(10-hexyl-10H-phenothiazin-3-yl)-3,6-dioxo-2,3,5,6-tetrahydropyrrolo[3,4-c]pyrrol-1-yl)-[1,1′-biphenyl]-4-yl)acrylic acid (**PTZ1**)*

A mixture of **11a** (240 mg, 0.31 mmol), *tert*-butyl cyanoacetate (0.089 mg, 0.63 mmol), ammonium acetate (48 mg, 0.63 mmol), and acetic acid (1 mL) in toluene (20 mL) was refluxed under argon atmosphere for 5 h. After cooling to room temperature, the reaction was quenched by water and the mixture was extracted with DCM. The organic layer was dried over anhydrous Na_2SO_4 and the solvent was removed by rotary evaporation. The crude product was further purified by column chromatography (silica gel, petroleum ether (bp 60–90 °C)/ethyl acetate = 20/1, v/v) to give **20a** as an aubergine solid. **20a** was hydrolyzed directly with trifluoroacetic acid (10 mL) under stirring at room temperature for 4 h. Deionized water (100 mL) was added to the mixture, and the resulting black solid was collected by filtration and washed by water to give **PTZ1** as a dark-red powder (mp 201–203 °C) in 73.9% yield for the two step reactions. ^{1}H NMR ($CDCl_3$, 400 MHz, ppm): δ 7.88–7.83 (m, 3H), 7.82–7.75 (m, 5H), 7.73–7.71 (m, 2H), 7.58–7.57 (m, 1H), 7.19–7.09 (m, 2H), 6.98–6.92 (m, 2H), 6.89–6.86 (m, 1H), 3.91–3.87 (m, 2H), 3.84–3.77 (m, 2H), 3.76–3.69 (m, 2H), 1.89–1.78 (m, 2H), 1.69–1.58 (m, 4H), 1.48–1.44 (m, 2H), 1.35–1.30 (m, 4H), 1.27–1.20 (m, 12H), 0.92–0.79 (m, 9H). ^{13}C NMR ($CDCl_3$, 100 MHz, ppm): δ 163.7, 163.0, 162.2, 153.5, 149.0, 148.1, 147.6, 143.6, 143.3, 140.8, 131.7, 131.0, 129.6, 129.1, 128.6, 127.6, 127.5, 127.4, 127.0, 126.9, 124.7, 123.7, 123.3, 121.6, 115.8, 115.7, 115.0, 109.8, 108.9, 102.8, 47.9, 42.4, 41.9, 31.4, 31.2, 31.2, 29.5, 29.3, 26.8, 26.6, 26.4, 22.6, 22.6, 22.5, 14.0, 14.0. HRMS (ESI, *m*/*z*): $[M + H]^+$ calcd for ($C_{52}H_{57}N_4O_4S$): 833.4095, found: 833.4088.

3. Result and discussion

3.1. Synthesis

Scheme 1 outlines the synthetic routes of the target dyes. 10-Hexyl-10*H*-phenothiazine-3-carbonitrile (**2**) and 4-(bis(4-(hexyloxy)phenyl)amino)benzonitrile (**4**) were synthesized from **1** and **3**, respectively, according to the methods reported in the literature [34]. They were reacted with **8** to yield **9a** and **9b**, respectively. Compounds **6**, **7**, **8**, **12** and **16** were obtained as reported earlier [35]. Introduction of an *n*-hexane chain on their **DPP** ring gave **10a**, **10b**, **13** and **17**, whose solubility were greatly enhanced. **11a**, **11b** and **18** were produced via the Suzuki coupling reaction of **10a**, **10b** and **17** with 4-formylphenylboronic acid in the presence of $Pd(PPh_3)_4$, 2 M aqueous solution of K_2CO_3, respectively. The hydrolysis reaction of **13** gave **14**. Another Suzuki coupling reaction was made with the corresponding bromides and (4-(bis(4-(hexyloxy)phenyl)amino) phenyl)boronic acid to afford **15a**, **15b**, **19a** and **19b**. Thereafter, the Knoevenagel condensation reactions of the aldehydes 1**1a**, **11b**, **15a**, **15b**, **19a** and **19b** with *tert*-butyl cyanoacetate in the presence of glacial acetic acid and ammonium acetate afforded the corresponding intermediates **20a**–**22b**. **20a** was hydrolyzed with trifluoroacetic acid to give **PTZ1**. Other five dyes were synthesized with the same procedure as that of **PTZ1**. The structures of the new key intermediates and six novel organic **DPP**-based sensitizers were confirmed by ^{1}H NMR, ^{13}C NMR and HRMS.

3.2. Photophysical properties

The UV–vis absorption spectra of the six dyes in CH_2Cl_2 (2×10^{-5} M) are depicted in Fig. 2a, and the corresponding photophysical data are summarized in Table 1. All the dyes show a broad absorption spectra with two typical absorption bands: one absorption peak in the ultraviolet region (300–380 nm) arising from the n–π^* and π–π^* transitions of the whole conjugation backbone, another one in the visible region (450–580 nm) corresponding to the intramolecular charge transfer (ICT) between the electron donor and acceptor moiety [36,37]. Interestingly, in the each type of the dyes, the maximum absorption wavelengths (λ_{max}) of the **PTZ**-based dyes (526 nm for **PTZ1**, 523 nm for **PTZ2** and 500 nm for **PTZ3**) are blue-shifted as compared to those of the **TPA**-based dyes (539 nm for **TPA1**, 536 nm for **TPA2** and 513 nm for **TPA3**). A similar result is found in the pioneer work [38]. A very similar absorption band between **PTZ1** and **PTZ2** as well as **TPA1** and **TPA2** suggests that the position of phenyl unit does not nearly influence the absorption range. Interestingly, the λ_{max} values of **Type 3** dyes are significantly blue-shifted than those of **Type 1** dyes, although the former have one additional phenyl ring. A possible explanation is that the additional phenyl unit twists the framework of the conjugation, which hinders the charge transfer from the donor to the acceptor moiety [39]. Furthermore, the highest molar extinction coefficients (ε_{max}) of the dyes decrease in the order of **TPA1** (34,480 M^{-1} cm^{-1}) > **TPA3** (33,360 M^{-1} cm^{-1}) > **TPA2** (27,480 M^{-1} cm^{-1}) > **PTZ1** (24,940 M^{-1} cm^{-1}) > **PTZ3** (21,240 M^{-1} cm^{-1}) > **PTZ2** (20,705 M^{-1} cm^{-1}). Accordingly, by incorporating the donor part directly to the **DPP** core, **Type 1** sensitizers represent better light-harvesting ability, such as wide absorption range and strong absorption strength, which may induce effective charge extraction and transfer, which can be

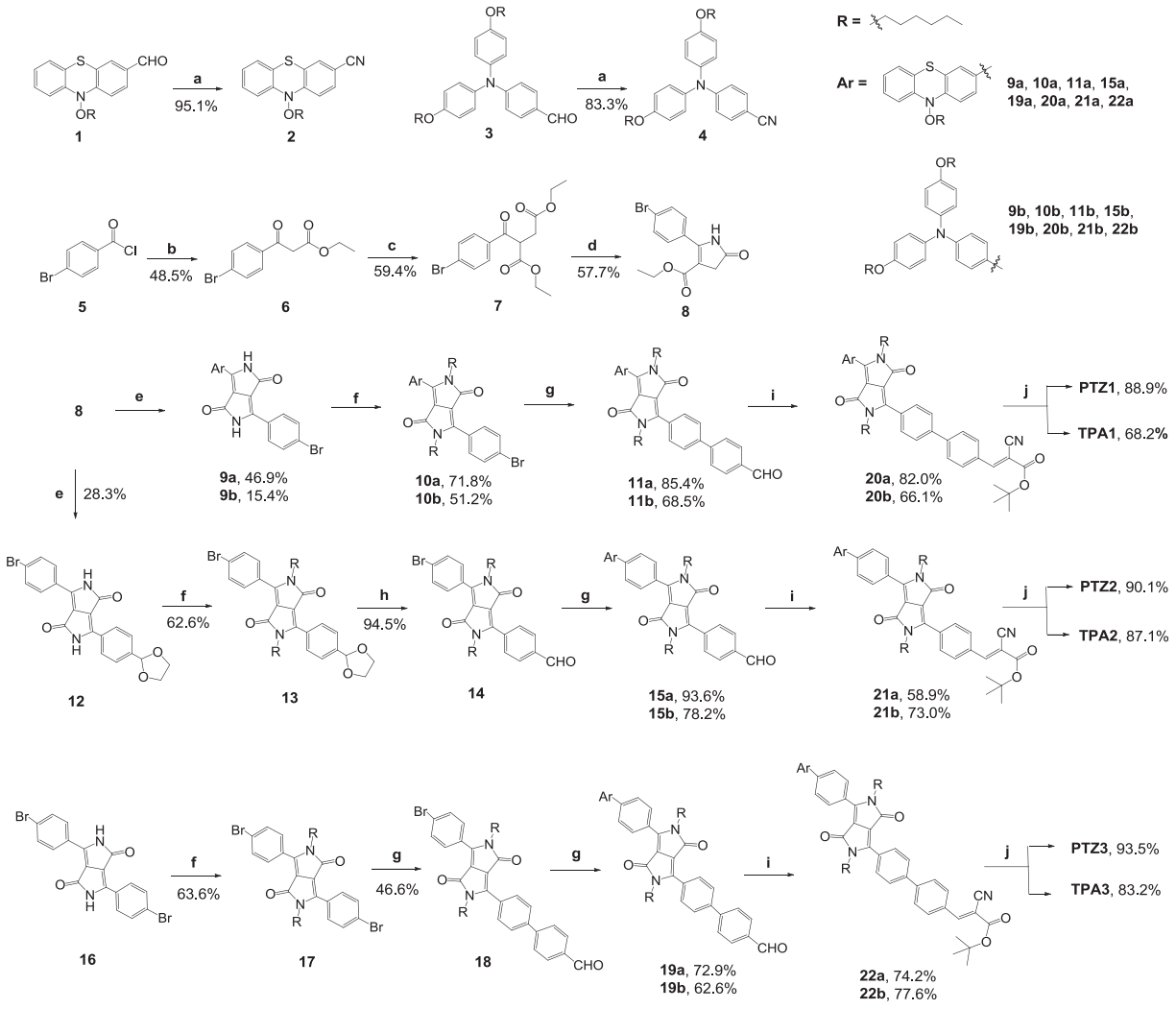

Scheme 1. Synthetic procedures of the dyes. Reagents and conditions: (a) Hydroxyamine hydrochloride, acetic acid, pyridine, DMF, Ar, 138 °C, 3.5 h; (b) Ethyl acetylacetate, NaOH (33%), petroleum ether, pH ≈ 11, 5 °C, 1 h; (c) Ethyl chloroacetace, K_2CO_3, KI, acetone, 1,2-dimethoxyethane, 75 °C, 20 h; (d) Ammonium acetate, acetic acid, N_2, 120 °C, 8 h; (e) Na, $FeCl_3$, *tert*-amyl alcohol, 4-(1,3-dioxolan-2-yl)benzonitrile or 10-hexyl-10*H*-phenothiazine-3-carbonitrile or 4-(bis(4-(hexyloxy)phenyl)amino)benzonitrile, N_2, 80 °C, 20 h; (f) Potassium *tert*-butanolate, 1-bromohexane, NMP, 60 °C, Ar, 24 h; (g) 4-Formylphenylboronic acid or (10-hexyl-10*H*-phenothiazin-3-yl)boronic acid or (4-(bis(4-(hexyloxy)phenyl) amino)phenyl)boronic acid, $Pd(PPh_3)_4$, 2 M aqueous solution of K_2CO_3, toluene, Ar, 80 °C, 24 h; (h) 2 M aqueous solution of hydrochloric acid, THF, 80 °C, 2 h; (i) *tert*-Butyl cyanoacetate, ammonium acetate, acetic acid, toluene, Ar, reflux for 5 h; (j) Trifluoroacetic acid, room temperature, 4 h.

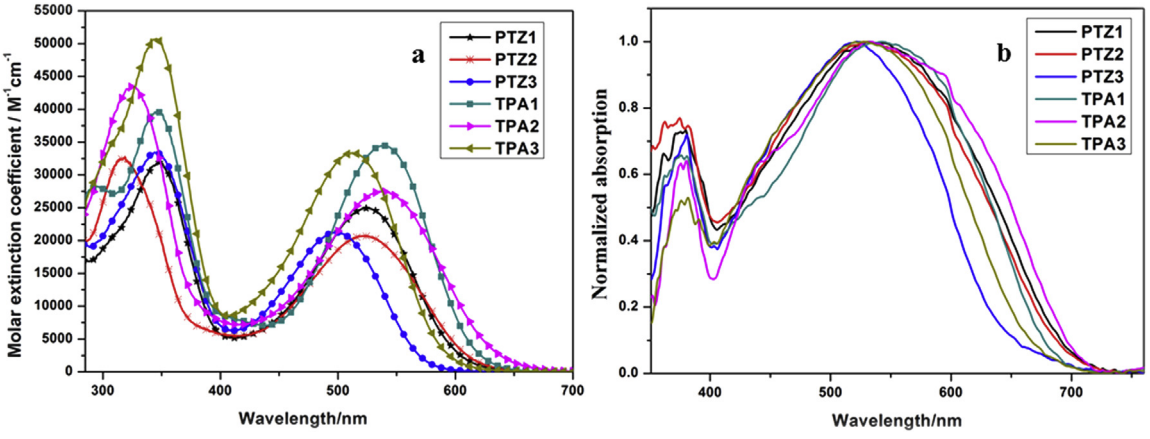

Fig. 2. Absorption spectra of the dyes in CH_2Cl_2 (a) and on TiO_2 film (b).

Table 1
Photochemical and electrochemical parameters of the dyes.

Dyes	λ_{max} (nm)/ (ε (M^{-1} cm^{-1}))[a]	λ_{max}(nm) (TiO_2)[b]	HOMO *vs* NHE (V)[c]	E_{0-0} (eV)[d]	LUMO *vs* NHE (V)[e]
PTZ1	348 (31,925) 526 (24,940)	532	0.86	2.10	−1.24
PTZ2	319 (32,685) 523 (20,705)	529	0.78	2.14	−1.36
PTZ3	347 (33,425) 500 (21,240)	521	0.73	2.31	−1.58
TPA1	346 (39,830) 539 (34,480)	543	0.88	2.04	−1.16
TPA2	326(43,520) 536 (27,480)	540	0.84	2.03	−1.21
TPA3	345 (50,730) 513 (33,360)	529	0.82	2.20	−1.36

[a] Absorption spectra in CH_2Cl_2 (2×10^{-5} M).
[b] Absorption maximum of the dyes anchored onto 12 μm TiO_2 films.
[c] HOMO was measured in acetonitrile with 0.1 M $TBAPF_6$ as electrolyte (scanning rate: 50 mv s^{-1}; working electrode and counter electrode: Pt wires; reference electrode: Ag/AgCl), Potentials measured *vs* Ag/AgCl were converted to NHE.
[d] E_{0-0} was determined from the intersection of the absorption and emission spectra in CH_2Cl_2.
[e] LUMO was calculated by HOMO − E_{0-0}.

confirmed entirely in the following density functional theory calculations. It should be mentioned that **TPA1** owns the highest molar extinction coefficient among these dyes, which will be in favor of enhancement of photocurrent generation in the DSSCs.

After anchored onto the TiO_2 films (Fig. 2b), the sensitizers **PTZ1**-**3** and **TPA1**-**3** show a bathochromic shift of 6, 6, 21, 4, 4 and 16 nm of the maximum absorption peaks in film with respect to their absorption spectra in solution, respectively. This red-shift hints that all these dyes behave *J*-aggregation on TiO_2 film, especially for **Type 3** dyes. The reason for the more serious *J*-aggregation of **Type 3** dyes is probably due to their expansion of π-conjugation. A trade-off of extending the π-conjugation readily causes π-stacked aggregation [6]. On account of the aggregation, the absorption spectra of the dyes become broad after adsorbed onto the semiconductor surface. In addition, it is found that the dyes with the **TPA** unit embody a slighter degree of aggregation than the dyes with **PTZ**, which is not only owing to the unique screw-like configuration of **TPA**, but also due to one more alkyl chain of **TPA** than **PTZ** [21,40].

3.3. Electrochemical properties

Cyclic voltammetry was performed to evaluate the possibilities of the electron transfer from the excited states of the dyes to the conduction band of TiO_2 (Table 1, Figs. 3 and 4). The oxidation potentials (E_{ox}) *vs* NHE corresponding to the HOMO levels of the dyes are 0.86 V for **PTZ1**, 0.78 V for **PTZ2**, 0.73 V for **PTZ3**, 0.88 V for **TPA1**, 0.84 V for **TPA2** and 0.82 V for **TPA3** versus NHE. As compared to **Type 2** dyes, a larger gap between the HOMO levels of **Type 1** dyes and I^-/I_3^- redox couple (0.42 V *vs* NHE) [41] is observed. It may imply that the oxidized dyes of **Type 1** dyes can be regenerated faster [42]. The energy gaps ($E_{0\text{-}0}$) of **PTZ1**–**3** and **TPA1**–**3** are 2.10, 2.14, 2.31, 2.04, 2.03 and 2.20 eV, respectively, which are estimated from the cross point of the normalized absorbance and emission spectra. The estimated excited state potential corresponding to the LUMO levels, calculated from HOMO − $E_{0\text{-}0}$, are −1.24, −1.36 and −1.58 V for **PTZ1**–**3**, while −1.16, −1.19 and −1.38 V for **TPA1**–**3** versus NHE, respectively. The data indicate that the efficient dye regeneration by I^-/I_3^- redox couple (0.42 V *vs* NHE), and the efficient electron injection into the TiO_2 conduction band (−0.50 V *vs.* NHE) are energetically possible for these sensitizers [43]. Apparently, as expected, the effect of the π-spacer on the HOMO and LUMO levels is remarkable in the metal free organic dyes.

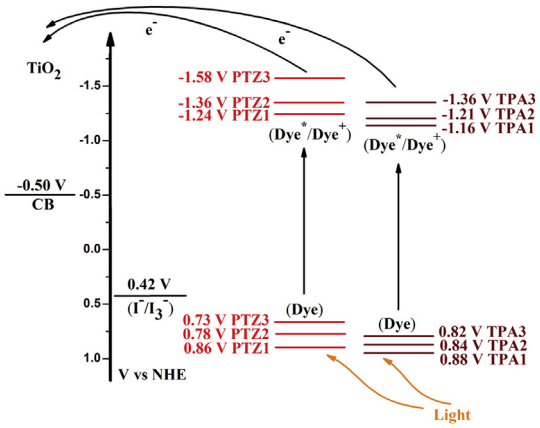

Fig. 3. HOMO/LUMO levels of the dyes.

3.4. Molecular orbital calculations

To gain insight into the molecular structure and electron distribution, the geometries of the dyes were optimized by the density functional theory (DFT) calculations at the B3LYP/6-31G* level with the Gaussian 03W program package [44]. The optimized structures and electronic distribution in the HOMO and LUMO levels are presented in Table 2. At the ground state (HOMO) of **Type 1** dyes, the electron distributions delocalize over the whole donor parts and **DPP** units and extend a little to the adjacent phenyl unit, while the LUMO orbitals show localized electron distribution throughout the entire A-π-A system part. For **Type 2** and **Type 3** sensitizers, the HOMO levels are blocked by the phenyl unit between the donor units and **DPP** units, which results in almost segregated electron distributions. As observed, their HOMO levels mainly concentrate on the donor segments with a very small fraction localized on the neighboring phenyl and **DPP** units. Correspondingly, the LUMO orbitals of these two types of molecules are delocalized over the **DPP** core, biphenyl unit and cyanoacrylic acid moiety. Hence, as compared to the other two types of the dyes, the electron communication of **Type 1** molecules may have a sufficient π-orbital overlap, allowing a more efficient shift of the electron from the electron donor moiety to the cyanoacrylic acid acceptor moiety [2,11]. From Table 2, it can also be seen that the phenyl unit arouses a twisted geometric structure of the dyes. Apparently, the nonplanar configurations are expected to suppress the aggregation and enhance the open-circuit voltage of the DSSCs.

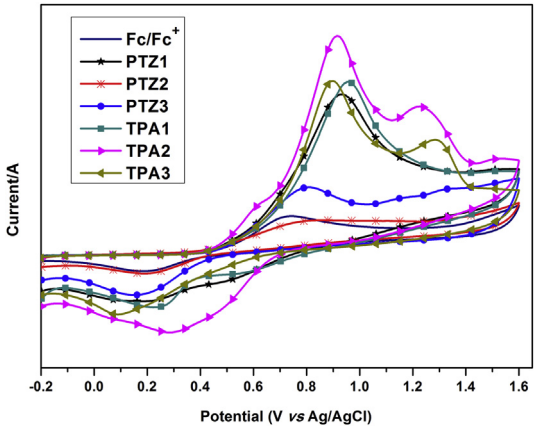

Fig. 4. Cyclic voltammetry of the dyes.

Table 2
Optimized structure and electron distribution in HOMO and LUMO levels of the dyes.

Dyes	Optimized structure	HOMO	LUMO
PTZ1	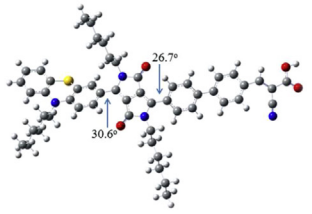	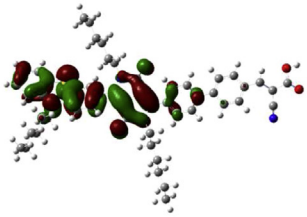	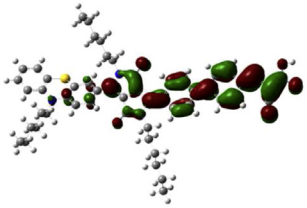
PTZ2	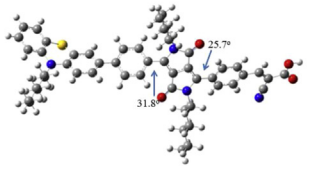	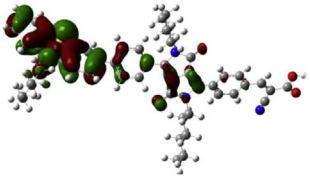	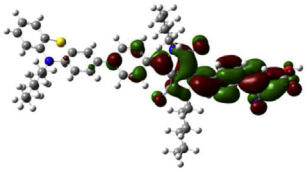
PTZ3	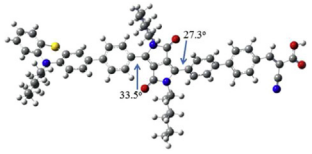	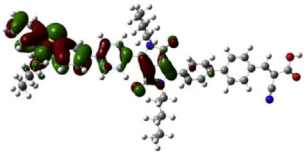	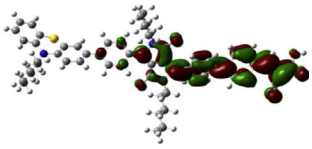
TPA1	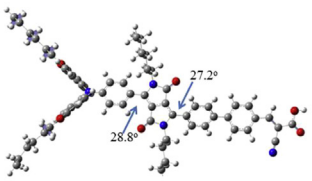	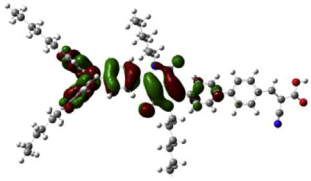	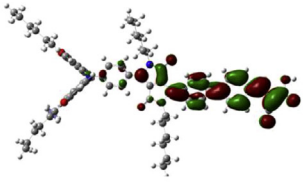
TPA2	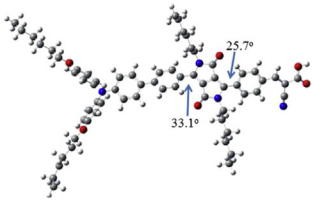	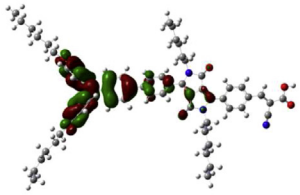	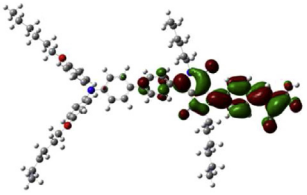
TPA3	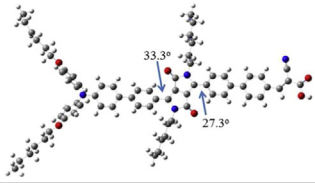		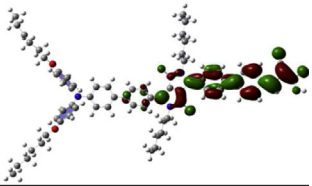

3.5. Photovoltaic performance of the DSSCs

Photovoltaic properties of the DSSC devices based on the dyes were studied and the detailed photovoltaic performance parameters are summarized in Table 3. The IPCE of the DSSCs exhibits broad spectral response range from 350 to 700 nm, indicating that these six dyes can efficiently convert the visible light into photocurrent (Fig. 5). Generally, in the each type of the dyes, the solar cells sensitized by the dyes with **TPA** as the electron donor unit have better performances than the dyes with **PTZ**. This result is in good agreement with the absorption performance of these dyes in solution (Fig. 2a). Typically, **TPA1** sensitized solar cell provides a plateaus of over 60% from 430 to 630 nm with the highest value of 67% at 530 nm and an onset at 800 nm, which demonstrates the capable wide-band spectral capture ability of this dye. On the other

Table 3
Photovoltaic parameters for the DSSCs.

Dyes	J_{sc}/mA cm^{-2}	V_{oc}/mV	ff	η/%
PTZ1[a]	11.65	656	0.68	5.16
PTZ2[a]	6.94	628	0.75	3.26
PTZ3[a]	9.68	638	0.74	4.56
TPA1[a]	15.50	730	0.67	7.57
TPA1[b]	15.40	717	0.72	7.96
TPA2[a]	7.51	645	0.85	4.12
TPA3[a]	13.43	699	0.65	6.06
N719[a]	16.72	774	0.68	8.83

[a] Without chenodeoxycholic acid (CDCA).
[b] 20 mM CDCA.

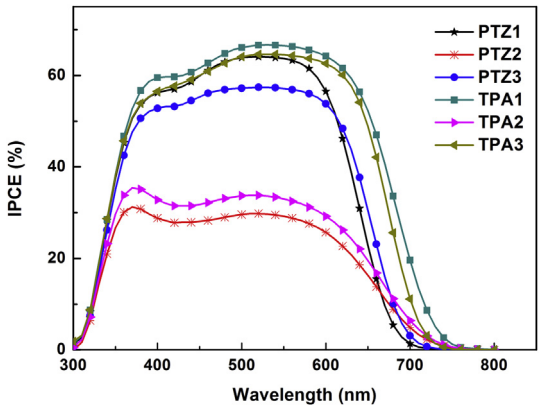

Fig. 5. IPCE of the DSSCs.

hand, the **PTZ1**, **PTZ2**, **PTZ3**, **TPA2** and **TPA3** sensitized cells deliver the highest IPCE values of 64% at 520 nm, 30% at 520 nm, 57% at 530 nm, 34% at 520 nm and 65% at 540 nm, respectively. The **TPA1** based DSSCs shows the best IPCE performance among the six dyes. It mainly originates from its wider absorption range, much higher molar extinction coefficient and faster regeneration of oxidized state [45]. Thus, it can be predicted that **TPA1** should present higher J_{sc} than the other dyes.

Photocurrent density–photovoltage (J–V) curves of the dyes were measured under the irradiation of AM 1.5 G full sunlight (Fig. 6). The detailed parameters of the short-circuit photocurrent density (J_{sc}), open-circuit photovoltage (V_{oc}), fill factor (ff) and photovoltaic conversion efficiency (η) are summarized in Table 3. The **TPA1**–**3** sensitized solar cells give a J_{sc} of 15.50, 7.51 and 13.43 mA cm^{-2}, a V_{oc} of 730, 645 and 699 mV, and a ff of 0.67, 0.85 and 0.65, corresponding to an overall conversion efficiency of 7.57, 4.02 and 6.06%, respectively. Under the same condition, the photovoltaic parameters (J_{sc}, V_{oc}, ff and η) of the cells sensitized by **PTZ1**–**3** are 11.65 mA cm^{-2}, 656 mV, 0.68 and 5.16%; 6.94 mA cm^{-2}, 628 mV, 0.75 and 3.26%; 9.68 mA cm^{-2}, 638 mV, 0.74 and 4.56%, respectively.

The value of J_{sc} is generated through light absorption, electron injection and dye regeneration [6]. In general, in the same type of the dyes, the dyes with **TPA** show better photovoltaic performance as compared to the dyes with **PTZ**, which may be due to a better photocurrent action spectra response. By linking the donor unit directly to the **DPP** moiety and shortening the electron transfer distance from the donor part to TiO_2, the charge extraction, transfer

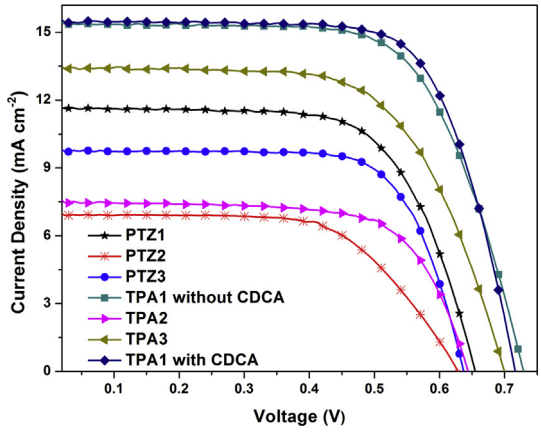

Fig. 6. J–V curves of the DSSCs sensitized by the dyes.

and electron injection may be promoted. As a result, the light collection capacity of **Type 1** sensitizers is the best among three types of the dyes, and then results in an obvious improvement of the photocurrents. Certainly, the oxidized **Type 1** dyes can be regenerated faster, which also contributes to a rise of J_{sc} value. On the other hand, **Type 2** and **Type 3** sensitizers exhibit relative moderate light collection capacity and lower delocalization of the excited state, which results in somewhat lower J_{sc} values. This phenomenon can be confirmed by the IPCE results.

The V_{oc} of the device is the potential difference between the quasi-Fermi level of TiO_2 and the redox potential of the applied electrolyte (I^-/I_3^-) [46,47], and is strongly influenced by the rate of electron recombination [48]. As discussed in the previous section, the asymmetric **DPP**-based dye **TPA1** with **TPA** as the donor unit exhibits the least extent of aggregation. Therefore, it may suppress I_3^- ions approaching to TiO_2 surface and restrain the dark current more efficiently, and thus yielding a higher V_{oc} value [47]. At the same time, **TPA1** displays the highest open-circuit voltage (730 mV) also due to the relative larger gap between its HOMO level and I^-/I_3^- redox couple, which leads to a faster regeneration of the oxidized dye [49].

On the basis of our design principle by introducing n-hexyl group on both the **DPP** and the electron donor unit as a barrier, as well as introducing phenyl unit as another π-bridge to minimize the planarity of the whole conjugation part of the dyes, it is expected to reduce the undesirable dye aggregation. However, the dye aggregation cannot be avoided completely. Thereby, **TPA1** is selected to be co-adsorbed with 20 mM chenodeoxycholic acid (CDCA). The efficiency of the DSSCs based on **TPA1** with 20 mM CDCA is up to 7.96% with a J_{sc} of 15.40 mA cm^{-2}, a V_{oc} of 717 mV and a fill factor of 0.72. This efficiency reaches about 90% of the efficiency of **N719**-based standard DSSC (8.83%) under the same conditions. As compared to the **TPA1**-based cell without CDCA, the J_{sc} and V_{oc} slightly decrease. The reason is that the amount of adsorbed dye molecules on TiO_2 surface is reduced by co-adsorption of CDCA, resulting in a loss of light harvesting units and decrease of the J_{sc} value [8]. At the same time, it was proved that a large amount of CDCA may leave protons on TiO_2 surface and then lead to a loss in V_{oc} [8,50]. Interestingly, the fill factor value increases, resulting in an enhancement of efficiency. Some similar results are found in the pioneer work [30,51]. In practice, its efficiency is only augmented nearly 5% even though the aggregation can usually be effectively suppressed by CDCA [52]. It also may imply that only a slight aggregation of **TPA1** molecules occurs.

3.6. Electrochemical impedance spectroscopy

The electrochemical impedance spectroscopy (EIS) was performed to elucidate the interfacial charge recombination process in the DSSCs. A typical Nyquist plot of the DSSCs in the dark (Fig. 7) displays three semicircles though it always reveals only first two semicircles [53]. The first semicircle observed at lower frequencies and the last one at higher frequencies correspond to the electron transport in the TiO_2 electrode and charge-transfer processes at the Pt/electrolyte interface, respectively. The middle major semicircle is ascribed to the electron recombination at the TiO_2/dye/electrolyte interface [53]. The radius of this semicircle is a measure of the charge recombination resistance (R_{rec}). A larger R_{rec} value indicates larger resistance for the related process. The R_{rec} value of the dyes decreases in the order of **TPA1** (42.9 Ω) > **TPA3** (37.6 Ω) > **PTZ1** (31.0 Ω) > **TPA2** (27.3 Ω) > **PTZ3** (24.8 Ω) > **PTZ2** (21.7 Ω), which suggests a trend of the lowest recombination rate in the order of **TPA1** < **TPA3** < **PTZ1** < **TPA2** < **PTZ3** < **PTZ2** [54]. In fact, the values of the electron recombination resistance of the dyes are well in accordance with the V_{oc} values.

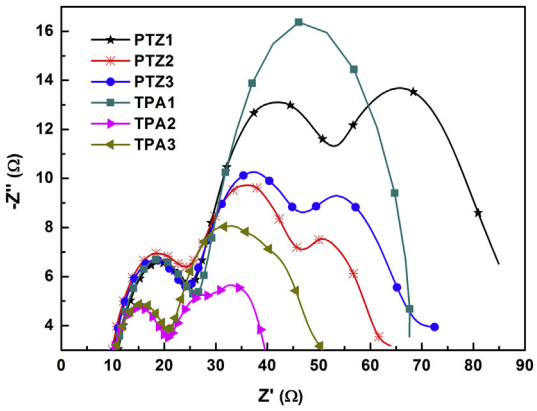

Fig. 7. EIS Nyquist plots of electrochemical impedance of the DSSCs sensitized by the dyes in dark conditions.

4. Conclusion

In summary, three types of **DPP-**based organic dyes (**Type 1**–**3**) were designed and synthesized for dye-sensitized solar cells. Among them, **Type 1** dyes present the best performance, while **Type 2** dyes are the poorest. The UV–vis absorption spectra, IPCE spectra and DFT calculation indicate that the charge extraction, transfer and electron injection processes are promoted by incorporating the donor part directly to the **DPP** core (**Type 1** sensitizers). **Type 1** dyes exhibit the strongest light collection capacity, most efficient charge transfer process and lowest aggregation trend. On the other hand, **Type 2** and **Type 3** dyes with a phenyl unit between the donor and **DPP** unit and a phenyl or biphenyl unit between the **DPP** and acceptor unit show lower power conversion efficiency because the delocalization of the excited state of the dyes is limited. The dyes with **TPA** as the donor unit behave the well matched energy levels, more excellent UV performance and smaller extent of aggregation than the dyes with **PTZ** as the donor unit. Under simulated AM 1.5 G solar light, **TPA1** sensitized cell device produces the best conversion efficiency of 8% with CDCA as the co-adsorbant. The results reveal that the donors, the position and number of phenyl unit significantly influence the photovoltaic performance of the dyes, which are helpful to design effective organic dyes for efficient DSSCs.

Acknowledgments

We are grateful to the National Natural Science Foundation of China (21272079), the Natural Science Foundation of Guangdong Province, China (10351064101000000, S2012010010634), the Fundamental Research Funds for the Central Universities (2014ZP0008) and the Fund from the Guangzhou Science and Technology Project, China (2012J4100003) for the financial support.

Appendix A. Supplementary data

Supplementary data related to this article can be found at http://dx.doi.org/10.1016/j.jpowsour.2014.08.030.

References

[1] B. O'Regan, M. Gratzel, Nature 353 (1991) 737–740.
[2] J. Luo, M. Xu, R. Li, K.-W. Huang, C. Jiang, Q. Qi, W. Zeng, J. Zhang, C. Chi, P. Wang, J. Wu, J. Am. Chem. Soc. 136 (2013) 265–272.
[3] B. Liu, W. Li, B. Wang, X. Li, Q. Liu, Y. Naruta, W. Zhu, J. Power Sources 234 (2013) 139–146.
[4] A. Mishra, M.K.R. Fischer, P. Bäuerle, Angew. Chem. Int. Ed. 48 (2009) 2474–2499.
[5] M. Liang, J. Chen, Chem. Soc. Rev. 42 (2013) 3453–3488.
[6] B.G. Kim, K. Chung, J. Kim, Chem.—Eur. J. 19 (2013) 5220–5230.
[7] W. Xu, B. Peng, J. Chen, M. Liang, F. Cai, J. Phys. Chem. C 112 (2008) 874–880.
[8] S. Qu, W. Wu, J. Hua, C. Kong, Y. Long, H. Tian, J. Phys. Chem. C 114 (2010) 1343–1349.
[9] Y. Jin, Y. Xu, Y. Liu, L. Wang, H. Jiang, X. Li, D. Cao, Dyes Pigm. 90 (2011) 311–318.
[10] J. Warnan, L. Favereau, Y. Pellegrin, E. Blart, D. Jacquemin, F. Odobel, J. Photochem. Photobiol. A: Chem. 226 (2011) 9–15.
[11] F. Zhang, K.-J. Jiang, J.-H. Huang, C.-C. Yu, S.-G. Li, M.-G. Chen, L.-M. Yang, Y.-L. Song, J. Mater. Chem. A 1 (2013) 4858–4863.
[12] S. Qu, C. Qin, A. Islam, Y. Wu, W. Zhu, J. Hua, H. Tian, L. Han, Chem. Commun. 48 (2012) 6972–6974.
[13] J.-H. Yum, T.W. Holcombe, Y. Kim, J. Yoon, K. Rakstys, M.K. Nazeeruddin, M. Gratzel, Chem. Commun. 48 (2012) 10727–10729.
[14] T.W. Holcombe, J.-H. Yum, Y. Kim, K. Rakstys, M. Gratzel, J. Mater. Chem. A 1 (2013) 13978–13983.
[15] S. Qu, B. Wang, F. Guo, J. Li, W. Wu, C. Kong, Y. Long, J. Hua, Dyes Pigm. 92 (2012) 1384–1393.
[16] T.W. Holcombe, J.-H. Yum, J. Yoon, P. Gao, M. Marszalek, D.D. Censo, K. Rakstys, M.K. Nazeeruddin, M. Graetzel, Chem. Commun. 48 (2012) 10724–10726.
[17] J. Tang, S. Qu, J. Hu, W. Wu, J. Hua, Sol. Energy 86 (2012) 2306–2311.
[18] Y. Wu, W. Zhu, Chem. Soc. Rev. 42 (2013) 2039–2058.
[19] Z. Hao, A. Iqbal, Chem. Soc. Rev. 26 (1997) 203–213.
[20] J. Zhao, X. Yang, M. Cheng, S. Li, X. Wang, L. Sun, J. Mater. Chem. A 1 (2013) 2441–2446.
[21] N. Koumura, Z.-S. Wang, S. Mori, M. Miyashita, E. Suzuki, K. Hara, J. Am. Chem. Soc. 128 (2006) 14256–14257.
[22] H. Zhang, J. Fan, Z. Iqbal, D.-B. Kuang, L. Wang, H. Meier, D. Cao, Org. Electron. 14 (2013) 2071–2081.
[23] Y. Hua, S. Chang, H. Wang, D. Huang, J. Zhao, T. Chen, W.-Y. Wong, W.-K. Wong, X. Zhu, J. Power Sources 243 (2013) 253–259.
[24] X.-F. Zang, T.-L. Zhang, Z.-S. Huang, Z. Iqbal, D.-B. Kuang, L. Wang, H. Meier, D. Cao, Dyes Pigm. 104 (2014) 89–96.
[25] Y. Hua, S. Chang, D. Huang, X. Zhou, X. Zhu, J. Zhao, T. Chen, W.-Y. Wong, W.-K. Wong, Chem. Mater. 25 (2013) 2146–2153.
[26] S. Chang, H. Wang, Y. Hua, Q. Li, X. Xiao, W.-K. Wong, W.Y. Wong, X. Zhu, T. Chen, J. Mater. Chem. A 1 (2013) 11553–11558.
[27] Y. Hua, S. Chang, J. He, C. Zhang, J. Zhao, T. Chen, W.Y. Wong, W.K. Wong, X. Zhu, Chem.—Eur. J. 20 (2014) 6300–6308.
[28] G. Wu, F. Kong, J. Li, X. Fang, Y. Li, S. Dai, Q. Chen, X. Zhang, J. Power Sources 243 (2013) 131–137.
[29] A. Hagfeldt, G. Boschloo, L. Sun, L. Kloo, H. Pettersson, Chem. Rev. 110 (2010) 6595–6663.
[30] Y. Hua, B. Jin, H. Wang, X. Zhu, W. Wu, M.-S. Cheung, Z. Lin, W.-Y. Wong, W.-K. Wong, J. Power Sources 237 (2013) 195–203.
[31] K.S.V. Gupta, T. Suresh, S.P. Singh, A. Islam, L. Han, M. Chandrasekharam, Org. Electron. 15 (2014) 266–275.
[32] L. Chen, X. Li, W. Ying, X. Zhang, F. Guo, J. Li, J. Hua, E. J. Org. Chem. 2013 (2013) 1770–1780.
[33] Z. Wu, Z. An, X. Chen, P. Chen, Org. Lett. 15 (2013) 1456–1459.
[34] N. Tamoto, C. Adachi, K. Nagai, Chem. Mater. 9 (1997) 1077–1085.
[35] Y. Xu, Y. Jin, W. Lin, J. Peng, H. Jiang, D. Cao, Synth. Met. 160 (2010) 2135–2142.
[36] X.-F. Zang, Y.-F. Xu, Z. Iqbal, Z.-S. Huang, D.-B. Kuang, L. Wang, H. Meier, Y. Li, D. Cao, Dyes Pigm. 99 (2013) 1072–1081.
[37] H.N. Tian, X.C. Yang, J.Y. Cong, R.K. Chen, C. Teng, J. Liu, Y. Hao, L. Wang, L.C. Sun, Dyes Pigm. 84 (2010) 62–68.
[38] J. Zhao, X. Yang, M. Cheng, S. Li, L. Sun, ACS Appl. Mater. Interfaces 5 (2013) 5227–5231.
[39] E.Q. Guo, P.H. Ren, Y.L. Zhang, H.C. Zhang, W.J. Yang, Chem. Commun. (2009) 5859–5861.
[40] C. Chen, X. Yang, M. Cheng, F. Zhang, J. Zhao, L. Sun, ACS Appl. Mater. Interfaces 5 (2013) 10960–10965.
[41] G.L. Zhang, Y. Bai, R.Z. Li, D. Shi, S. Wenger, S.M. Zakeeruddin, M. Gratzel, P. Wang, Energy Environ. Sci. 2 (2009) 92–95.
[42] J. Heo, J.W. Oh, H.I. Ahn, S.B. Lee, S.E. Cho, M.R. Kim, J.K. Lee, N. Kim, Synth. Met. 160 (2010) 2143–2150.
[43] M. Gratzel, Nature 414 (2001) 338–344.
[44] M.J. Frisch, G.W. Trucks, H.B. Schlegel, P.M.W. Gill, B.G. Johnson, M.A. Robb, J.R. Cheeseman, T. Keith, G.A. Petersson, J.A. Montgomery, K. Raghavachari, M.A. Al-Laham, V.G. Zakrzewski, J.V. Ortiz, J.B. Foresman, J. Cioslowski, B.B. Stefanov, A. Nanayakkara, M. Challacombe, C.Y. Peng, P.Y. Ayala, W. Chen, M.W. Wong, J.L. Andres, E.S. Replogle, R. Gomperts, R.L. Martin, D.J. Fox, J.S. Binkley, D.J. Defrees, J. Baker, J.P. Stewart, M. Head-Gordon, C. Gonzalez, J.A. Pople, Gaussian 03, Revision E.01, Gaussian, Inc., Pittsburgh, PA, 2004.
[45] W. Wu, J. Zhang, H. Yang, B. Jin, Y. Hu, J. Hua, C. Jing, Y. Long, H. Tian, J. Mater. Chem. 22 (2012) 5382–5389.
[46] S. Kajiyama, Y. Uemura, H. Miura, K. Hara, N. Koumura, Dyes Pigm. 92 (2012) 1250–1256.
[47] T. Marinado, K. Nonomura, J. Nissfolk, M.K. Karlsson, D.P. Hagberg, L.C. Sun, S. Mori, A. Hagfeldt, Langmuir 26 (2010) 2592–2598.

[48] Y. Zhang, Y. Zhang, Z. Wang, M. Liang, D. Jia, Q. Wu, S. Xue, J. Power Sources 253 (2014) 167–176.
[49] Z. Ning, Y. Fu, H. Tian, Energy Environ. Sci. 3 (2010) 1170–1181.
[50] N.R. Neale, N. Kopidakis, J. van de Lagemaat, M. Grätzel, A.J. Frank, J. Phys. Chem. B 109 (2005) 23183–23189.
[51] W. Li, Y. Wu, X. Li, Y. Xie, W. Zhu, Energy Environ. Sci. 4 (2011) 1830–1837.
[52] M. Guo, P. Diao, Y.-J. Ren, F. Meng, H. Tian, S.-M. Cai, Sol. Energy Mater. Sol. Cells 88 (2005) 23–35.
[53] A. Baheti, K.R. Justin Thomas, C.-P. Lee, C.-T. Li, K.-C. Ho, J. Mater. Chem. A 2 (2014) 5766–5779.
[54] Y.J. Chang, T.J. Chow, J. Mater. Chem. 21 (2011) 9523–9531.